The Astrophysical Journal, 596:847–859, 2003 October 20

COORDINATED MULTIWAVELENGTH OBSERVATIONS OF BL LACERTAE IN 2000

M. Böttcher,[1] A. P. Marscher,[2] M. Ravasio,[3] M. Villata,[4] C. M. Raiteri,[4] H. D. Aller,[5] M. F. Aller,[5] H. Teräsranta,[6] O. Mang,[7] G. Tagliaferri,[3] F. Aharonian,[8] H. Krawczynski,[9] O. M. Kurtanidze,[10,11,12] M. G. Nikolashvili,[10] M. A. Ibrahimov,[13,14] I. E. Papadakis,[15,16] K. Tsinganos,[15] K. Sadakane,[17] N. Okada,[17] L. O. Takalo,[18] A. Sillanpää,[18] G. Tosti,[19] S. Ciprini,[19] A. Frasca,[20] E. Marilli,[20] R. Robb,[21] J. C. Noble,[22] S. G. Jorstad,[22] V. A. Hagen-Thorn,[23] V. M. Larionov,[24] R. Nesci,[25] M. Maesano,[25] R. D. Schwartz,[26] J. Basler,[26] P. W. Gorham,[27] H. Iwamatsu,[28] T. Kato,[28] C. Pullen,[29] E. Benítez,[30] J. A. de Diego,[30] M. Moilanen,[31] A. Oksanen,[31] D. Rodriguez,[32] A. C. Sadun,[33] M. Kelly,[33] M. T. Carini,[34] H. R. Miller,[35] S. Catalano,[20] D. Dultzin-Hacyan,[30] J. H. Fan,[23] G. Ghisellini,[3] R. Ishioka,[28] H. Karttunen,[18] P. Keinänen,[18] N. A. Kudryavtseva,[24] M. Lainela,[18] L. Lanteri,[4] E. G. Larionova,[24] K. Matsumoto,[28] J. R. Mattox,[36] I. McHardy,[37] F. Montagni,[25] G. Nucciarelli,[19] L. Ostorero,[38] J. Papamastorakis,[15,16] M. Pasanen,[18] G. Sobrito,[4] and M. Uemura[28]

Received 2003 June 9; accepted 2003 June 30

ABSTRACT

BL Lacertae (BL Lac) was the target of an extensive multiwavelength monitoring campaign in the second half of 2000. Simultaneous or quasi-simultaneous observations were taken at radio (University of Michigan Radio Astronomy Observatory and Metsähovi Radio Telescope) and optical (Whole Earth Blazar Telescope [WEBT] collaboration) frequencies, in X-rays (*BeppoSAX* and *RXTE*), and at very high energy gamma rays (HEGRA). The WEBT optical campaign achieved an unprecedented time coverage, virtually continuous over several 10–20 hr segments. It revealed intraday variability on timescales of $\sim$1.5 hr and evidence for spectral hardening associated with increasing optical flux. During the campaign, BL Lac underwent a major transition from a rather quiescent state prior to 2000 September, to a flaring state for the rest of the year. This

[1] Department of Physics and Astronomy, Clippinger 339, Ohio University, Athens, OH 45701.
[2] Department of Astronomy, Boston University, 725 Commonwealth Avenue, Boston, MA 02215.
[3] Osservatorio Astronomico di Brera, Via Bianchi 46, I-23807 Merate, Italy.
[4] Istituto Nazionale di Astrofisica (INAF), Osservatorio Astronomico di Torino, Via Osservatorio 20, I-10025 Pino Torinese, Italy.
[5] Department of Astronomy, University of Michigan, 810 Dennison Building, Ann Arbor, MI 48109-1090.
[6] Metsähovi Radio Observatory, Helsinki University of Technology, Metsähovintie 114, 02540 Kylmälä, Finland.
[7] Institut für Experimentelle und Angewandte Physik, Universität Kiel, Leibnitzstrasse 15–19, D-24118 Kiel, Germany.
[8] Max-Planck-Institut für Kernphysik, Postfach 10 39 80, D-69029 Heidelberg, Germany.
[9] Physics Department, Washington University, 1 Brookings Drive, CB 1105, St. Louis, MO 63130.
[10] Abastumani Observatory, 383762 Abastumani, Georgia.
[11] Astrophysikalisches Institute Potsdam, An der Sternwarte 16, D-14482 Potsdam, Germany.
[12] Landessternwarte Heidelberg-Königstuhl, Königstuhl 12, D-69117 Heidelberg, Germany.
[13] Ulugh Beg Astronomical Institute, Uzbek Academy of Sciences, Astronomicheskaya 33, Tashkent 700052, Uzbekistan.
[14] Isaac Newton Institute of Chile, Uzbekistan Branch.
[15] Physics Department, University of Crete, 710 03 Heraklion, Crete, Greece.
[16] IESL, Foundation for Research and Technology-Hellas, 711 10 Heraklion, Crete, Greece.
[17] Astronomical Institute, Osaka Kyoiku University, Kashiwara-shi, Osaka 582-8582, Japan.
[18] Tuorla Observatory, 21500 Piikkiö, Finland.
[19] Osservatorio Astronomico, Università di Perugia, Via B. Bonfigli, I-06126 Perugia, Italy.
[20] Osservatorio Astrofisico di Catania, Viale A. Doria 6, I-95125 Catania, Italy.
[21] Department of Physics and Astronomy, University of Victoria, BC, Canada.
[22] Institute for Astrophysical Research, Boston University, 725 Commonwealth Avenue, Boston, MA 02215.
[23] Center for Astrophysics, Guangzhou University, Guangzhou 510400, China.
[24] Astronomical Institute, St. Petersburg State University, Bibliotechnaya Pl. 2, Petrodvoretz, 198504 St. Petersburg, Russia.
[25] Dipartimento di Fisica, Università La Sapienza, Piazzale A. Moro 2, I-00185 Rome, Italy.
[26] Department of Physics and Astronomy, University of Missouri-St. Louis, 8001 Natural Bridge Road, St. Louis, MO 63121.
[27] Jet Propulsion Laboratory, California Institute of Technology, 4800 Oak Grove Drive, Pasadena, CA 91109.
[28] Department of Astronomy, Faculty of Science, Kyoto University, Kyoto, Japan.
[29] Clarke and Coyote Astrophysical Observatory, P.O. Box 930, Wilton, CA 95693.
[30] Instituto de Astronomía, UNAM, Apartado Postal 70-264, 04510 Mexico DF, Mexico.
[31] Nyrölä Observatory, Jyväskylän Sirius ry, Kyllikinkatu 1, 40950 Jyväskylä, Finland.
[32] Guadarrama Observatory, C/ San Pablo 5, Villalba 28409, Madrid, Spain.
[33] Department of Physics, University of Colorado, P.O. Box 173364, Denver, CO 80217-3364.
[34] Department of Physics and Astronomy, Western Kentucky University, 1 Big Red Way, Bowling Green, KY 42104.
[35] Department of Physics and Astronomy, Georgia State University, Atlanta, GA 30303.
[36] Department of Chemistry, Physics, and Astronomy, Francis Marion University, P.O. Box 100547, Florence, SC 29501-0547.
[37] Department of Physics and Astronomy, University of Southampton Highfield, Southampton SO17 1BJ, UK.
[38] Dipartimento di Fisica Generale, Università di Torino, Via P. Giuria 1, I-10125 Turin, Italy.

was also evident in the X-ray activity of the source. *BeppoSAX* observations on July 26–27 revealed a rather low X-ray flux and a hard spectrum, while a *BeppoSAX* pointing on 2000 October 31–November 2 indicated significant variability on timescales of $\lesssim$a few hours and provided evidence for the synchrotron spectrum extending out to $\sim$10 keV during that time. During the July 26–27 observation, there is a tantalizing, although not statistically significant, indication of a time delay of $\sim$4–5 hr between the *BeppoSAX* and the *R*-band light curves. Also, a low-significance detection of a time delay of 15 days between the 14.5 and 22 GHz radio light curves is reported. Several independent methods to estimate the comoving magnetic field in the source are presented, suggesting a value of $\sim 2 e_B^{2/7}$ G, where e_B is the magnetic field equipartition factor with respect to the electron energy density in the jet.

Subject headings: BL Lacertae objects: individual (BL Lacertae) — galaxies: active — gamma rays: theory — radiation mechanisms: nonthermal

On-line material: color figure

1. INTRODUCTION

BL Lacertae (=1ES 2200+420; $z = 0.069$) was historically the prototype of the BL Lac class of active galactic nuclei (AGNs). These objects are characterized by continuum properties similar to those of flat-spectrum radio quasars (FSRQs; nonthermal optical continuum, high degree of linear polarization, rapid variability at all wavelengths, radio jets with individual components often exhibiting apparent superluminal motion) but usually show only weak emission or absorption lines (with equivalent width in the rest frame of the host galaxy of <5 Å), if any. In BL Lac itself, however, Hα (and Hβ) emission lines have been detected during a period of several weeks in 1995 (Vermeulen et al. 1995; Corbett et al. 1996) and in 1997 (Corbett et al. 2000). Superluminal motion of $\beta_{\rm app}$ up to $(5.0 \pm 0.2)\, h^{-1} \approx (7.1 \pm 0.3)$ has been observed in this object (Denn, Mutel, & Marscher 2000).

BL Lac objects and FSRQs are commonly unified in the AGN class of blazars. Sixty-five blazars have been detected and identified with high confidence in high-energy (>100 MeV) gamma rays by the EGRET instrument on board the *Compton Gamma Ray Observatory* (Hartman et al. 1999; Mattox, Hartman, & Reimer 2001). To date, six blazars have been detected at very high energies (>300 GeV) with ground-based air Cerenkov detectors (Punch et al. 1992; Quinn et al. 1996; Catanese et al. 1998; Chadwick et al. 1999; Aharonian et al. 2002; Horan et al. 2002; Holder et al. 2003). All of these belong to the subclass of high-frequency peaked BL Lac objects (HBLs). The field of extragalactic GeV–TeV astronomy is currently one of the most rapidly expanding research areas in astrophysics. The steadily improving flux sensitivities of the new generation of air Cerenkov telescope arrays and their decreasing energy thresholds (for a recent review see, e.g., Weekes et al. 2002), provide a growing potential to extend their extragalactic-source list toward intermediate and even low-frequency peaked BL Lac objects (LBLs) with lower νF_ν peak frequencies in their broadband spectral energy distributions (SEDs). Detection of such objects at energies $\sim$40–100 GeV might provide an opportunity to probe the intrinsic high-energy cutoff of their SEDs, since at those energies, γ-γ absorption due to the intergalactic infrared background is still expected to be negligible at redshifts of $z \lesssim 0.2$ (de Jager & Stecker 2002). There has even been a claimed detection of BL Lac in 1998 with the Cerenkov telescope of the Crimean Astrophysical Observatory (Neshpor et al. 2001); however, this detection could not be confirmed by any other group so far (e.g., Aharonian et al. 2000).

BL Lac is classified as an LBL. From an interpolation between the GHz radio spectrum and the IR–optical spectrum, it can be inferred that its low-frequency spectral component typically peaks at millimeter to micron wavelengths, while the high-frequency component seems to peak in the multi-MeV–GeV energy range. BL Lac has been the target of many radio, optical, X-ray, and gamma-ray observations in the past and has been studied in detail during various intensive multiwavelength campaigns (see, e.g., Bloom et al. 1997; Sambruna et al. 1999; Madejski et al. 1999; Ravasio et al. 2002; M. Villata et al. 2003, in preparation). It is a particularly interesting object for detailed X-ray studies: this is the region of the electromagnetic spectrum where the two broad components of the multiwavelength SEDs of BL Lac (and other LBLs) are overlapping and intersecting. X-ray observations of this source at different epochs show significant flux and spectral variability, indicating that the X-ray emission is at times dominated by the high-energy end of the synchrotron emission, while at other occasions it is dominated by the low-frequency portion of the high-energy bump of the SED. In fact, BL Lac has repeatedly shown a concave shape (see, e.g., Madejski et al. 1999; Ravasio et al. 2002), with rapid variability mainly restricted to the low-energy excess portion of the spectrum (see, e.g., Ravasio et al. 2002, 2003).

In the framework of relativistic jet models, the low-frequency (radio–optical/UV) emission from blazars is interpreted as synchrotron emission from nonthermal electrons in a relativistic jet. The high-frequency (X-ray–gamma-ray) emission could be produced either via Compton upscattering of low-frequency radiation by the same electrons responsible for the synchrotron emission (leptonic jet models; for a recent review see, e.g., Böttcher 2002), or because of hadronic processes initiated by relativistic protons co-accelerated with the electrons (hadronic models, for a recent discussion see, e.g., Mücke & Protheroe 2001; Mücke et al. 2003).

While simultaneous broadband spectra are very useful to constrain blazar jet models, there still remain severe ambiguities in their interpretation with respect to the dominant electron cooling, injection, and acceleration mechanisms, as very drastically illustrated for the case of W Comae by Böttcher, Mukherjee, & Reimer (2002). Those authors have also demonstrated that a combination of broadband spectra with timing and spectral variability information, in tandem with time-dependent model simulations (e.g., Böttcher & Chiang 2002; Krawczynski, Coppi, & Aharonian 2002), can help to break some of these degeneracies. For this reason, we organized an intensive multiwavelength campaign to

observe BL Lac in the second half of 2000 at as many frequencies as possible, putting special emphasis on detailed variability information. In § 2, we describe the observations carried out during the campaign and present light curves in the various energy bands. The diverse spectral variability patterns are discussed in § 3, and the results of our search for interband cross-correlations and time lags are presented in § 4. The source underwent a dramatic state transition, from a rather quiescent state until the middle of 2000 September, to a very active state that lasted throughout the remainder of the year. We have obtained two detailed simultaneous broadband spectra of BL Lac, one before and one after this transition. The resulting SEDs are presented in § 5. In § 6 we use our results to derive estimates of generic model parameters, in particular of the comoving magnetic field, independent of the details of any specific model. In a companion paper (M. Böttcher & A. Reimer 2003, in preparation), we will use leptonic and hadronic models to fit the spectra and variability patterns found in this campaign. We summarize in § 7.

Throughout this paper, we refer to α as the energy spectral index, F_ν [Jy] $\propto \nu^{-\alpha}$. A cosmology with $\Omega_m = 0.3$, $\Omega_\Lambda = 0.7$, and $H_0 = 70$ km s^{-1} Mpc^{-1} is used.

2. OBSERVATIONS, DATA REDUCTION, AND LIGHT CURVES

BL Lac was observed in a coordinated multiwavelength campaign at radio, optical, X-ray, and very high energy (VHE) gamma-ray energies during the period from mid-May of 2000 until the end of the year. The overall timeline of the campaign, along with the measured long-term light curves at radio, optical, and X-ray frequencies, is illustrated in Figure 1.

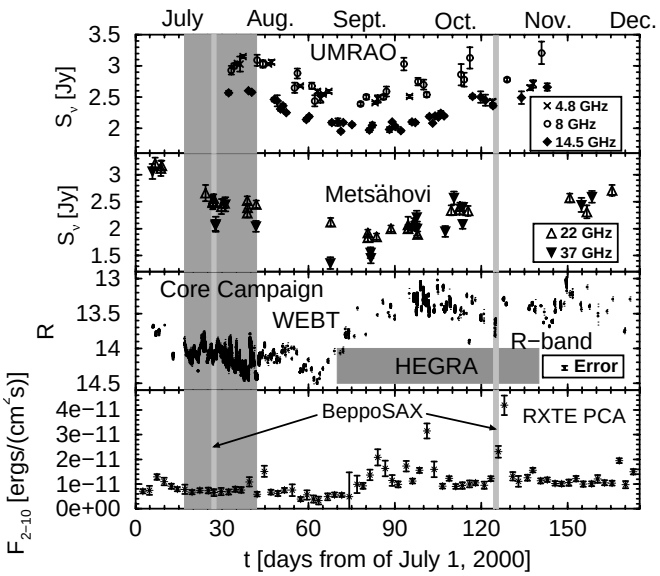

FIG. 1.—Timeline of the broadband campaign on BL Lac in 2000. The dark shaded areas indicate the duration of the core campaign, 2000 July 17–August 11, and of the HEGRA observations (collecting a total of 10.5 hr of on-source time); the light shaded areas indicate the times of our two *BeppoSAX* pointings. For clarity, the error bars on the *R*-band magnitudes have not been plotted individually. The inset in the lower right-hand corner of the third panel shows the typical error bar for measurements outside the core campaign; the errors are typically a factor of 3 smaller than this during the core campaign.

2.1. *Radio Observations*

At radio frequencies, the object was monitored using the University of Michigan Radio Astronomy Observatory (UMRAO) 26 m telescope, at 4.8, 8, and 14.5 GHz, and the 14 m Metsähovi Radio Telescope of Helsinki University of Technology, at 22 and 37 GHz. The radio light curves are shown in the top two panels of Figure 1. At the lower frequencies (4.8, 8, and 14.5 GHz), they show evidence for flux variability on a ~30% level on timescales of ~1 month and track each other closely. Superposed on the large-amplitude variability on a ~1 month timescale, the 4.8 and 8 GHz radio light curves exhibit low-amplitude variability on timescales of a few days. The discrete autocorrelation functions (ACFs; Edelson & Krolik 1988) of these light curves indicate a sharp decline on a timescale of ~4 days.

The higher frequency radio light curves indicate more erratic variability, with flux variations of ~25% within a few days. However, those variability patterns are clearly undersampled in our data set, so that a more detailed analysis might not be meaningful at this point.

2.2. *Optical Observations*

Focusing on an originally planned core campaign period of July 17–August 11, BL Lac was the target of an intensive optical campaign by the Whole Earth Blazar Telescope (WEBT; Villata et al. 2000; Raiteri et al. 2001),[39] in which 24 optical telescopes throughout the northern hemisphere participated. Details of the data collection, analysis, cross-calibration of photometry from different observatories, etc., pertaining to the WEBT campaign have been published in Villata et al. (2002). Observations were made in the standard *U*, *B*, *V*, *R*, and *I* bands. For the purpose of broadband spectroscopy, the fluxes were corrected for extinction and reddening using a *B*-band extinction value of $A_B = 1.42$ (Schlegel, Finkbeiner, & Davis 1998) and the extinction law of Cardelli, Clayton, & Mathis (1989). The contribution of the host galaxy was subtracted as described in detail in Villata et al. (2002).

Figure 1 illustrates that BL Lac was in a rather quiescent state during the core campaign, in which the densest light-curve sampling was obtained. However, the source underwent a dramatic state transition to an extended high state in mid-September of 2000. For this reason, the WEBT campaign was extended until early 2001 January, although with less dense time coverage than during the core campaign.

The WEBT campaign returned optical (*R*-band) light curves of unprecedented time coverage and resolution. Figure 2 shows the *R*-band light curves over the entire core campaign (see also Fig. 2 of Villata et al. 2002). The bottom panel of Figure 11 (see also Figs. 3–5 of Villata et al. 2002) illustrates the microvariability measured for two individual nights during this period. Brightness variations of $\Delta R \sim 0.35$, corresponding to flux variations of $(\Delta F)/F \sim 0.4$, within ~1.5 hr have been found. Such rapid microvariability is not exceptional for this source and had been observed before on several occasions (e.g., Miller, Carini, & Goodrich 1989; Carini et al. 1992; Nesci et al. 1998; Speziali & Natali 1998; Clements & Carini 2001). It is also confirmed by the ACF of the *R*-band light curve, which can be well fitted with an exponential with a decay timescale of ~2 hr. The observed

[39] See also http://www.to.astro.it/blazars/webt.

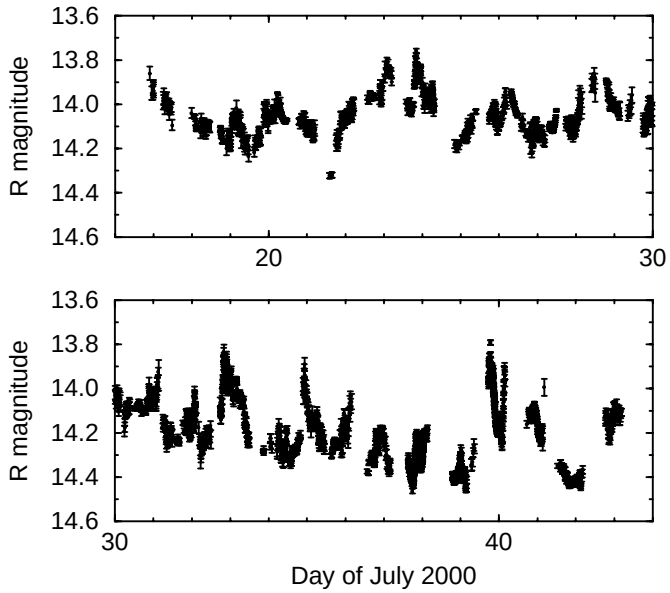

FIG. 2.—Optical (*R*-band) light curve of BL Lac during the core campaign of 2000 July 17–August 11 (Villata et al. 2002).

variability timescale places a constraint on the size of the emitting region of $R \lesssim 1.6 \times 10^{14} D$ cm, where $D = [\Gamma(1 - \beta \cos \theta_{\rm obs})]^{-1}$ is the Doppler beaming factor.

2.3. *X-Ray Observations*

At X-ray energies, BL Lac was observed with the *BeppoSAX* narrow field instruments (NFI) in the energy range 0.1–200 keV in two pointings on 2000 July 26–27 and October 31–November 2 (Ravasio et al. 2003). In addition, the source was monitored by the *Rossi X-Ray Timing Explorer* (*RXTE*) Proportional Counter Array (PCA) in three short (individual exposures ranging from a few hundred to ~2000 s) pointings per week (A. P. Marscher et al. 2003, in preparation). Table 1 summarizes the precise times of the two *BeppoSAX* pointings and of the *RXTE* PCA observations closest to the *BeppoSAX* ones, along with the results of the spectral analysis. The details of the *BeppoSAX* observations and the data analysis methods have been published in Ravasio et al. (2003). Note that the PCA had observed BL Lac exactly simultaneously with the *BeppoSAX* pointing during the July 26–27 observation, while an observation on November 2 started 1 hr after the second *BeppoSAX* pointing.

The drastic change of the activity state of BL Lac in mid-September observed in the optical range is accompanied by several large flares in the PCA light curve over a ~2 month period (see Fig. 1) but not by a similarly extended high flux state as seen in the optical. In fact, while the average flux level increased only slightly, a higher level of activity was indicated by a higher degree of variability: The average PCA 2–10 keV flux increased from 7.1×10^{-12} ergs cm^{-2} s^{-1} for the period MJD 51725–51795 (end of 2000 June to early September) to 1.2×10^{-11} ergs cm^{-2} s^{-1} for the period MJD 51800–51910 (middle of 2000 September to end of December). A constant fit to the quiescent phase resulted in a reduced $\chi^2_\nu = 3.47$, which increased to $\chi^2_\nu = 6.63$ for the remainder of the year. This quantifies the drastically increased 2–10 keV X-ray variability on timescales of a few days probed by the PCA monitoring observations, in the active state. However, it also shows that BL Lac exhibits significant X-ray variability on this timescale even in the quiescent state.

Figure 1 also shows that we were extremely lucky to catch BL Lac in an exceptional X-ray outburst during our second *BeppoSAX* pointing. In fact, the 2–10 keV flux measured on 2000 October 31–November 2 was the highest ever detected by *BeppoSAX* from this source. Interestingly, the *R*-band light curve indicates a relatively low optical flux, compared to the average flux level after mid-September of 2000, coincident with this X-ray outburst. If the optical and soft X-ray fluxes are due to synchrotron emission from the same population of electrons, this could indicate a hardening of the electron spectrum during the flaring state. However, as pointed out and discussed by Ravasio et al. (2003) and in § 5, the optical and X-ray spectra during this observation cannot be connected by a smooth power law: the optical fluxes are significantly below a power-law extrapolation of the *BeppoSAX* LECS+MECS spectrum. This could possibly indicate that the optical and X-ray fluxes are coming from separate regions along the jet, possibly also associated with substantial time lags between these emissions.

2.3.1. *July 26–27*

During the July 26–27 *BeppoSAX* observation, the source was in a low flux and activity state. This only allowed a rather restricted spectral analysis and the extraction of meaningful light curves with a binning of no less than 1 hr. For details of the spectral and timing analysis, see Ravasio et al. (2003). They tested several spectral models, including a single power law with free $N_{\rm H}$, a single power law with a fixed value of $N_{\rm H}$, and a broken–power-law model. In the following, we concentrate on the results from the analysis with $N_{\rm H} = 2.5 \times 10^{21}$ cm^{-2}, resulting from the dust-to-gas ratio suggested by Ryter (1996) with $A_B = 1.42$ and the dereddening law as mentioned in § 2.2 and consistent with

TABLE 1

SUMMARY OF X-RAY (*RXTE* PCA AND *BeppoSAX* MECS) OBSERVATIONS AND SPECTRAL ANALYSIS RESULTS FOR A SINGLE–POWER-LAW MODEL WITH FIXED $N_{\rm H} = 2.5 \times 10^{21}$ CM^{-2}

Instrument	Start Time (UT)	End Time (UT)	Duration (s)	α	$F_{1\,\rm keV}$ (μJy)	$F_{2-10\,\rm keV}$ (10^{-12} ergs s^{-1} s^{-2})	χ^2_ν/dof
PCA	Jul 26, 18:23:44	Jul 26, 19:00:32	2208	$0.9^{+0.7}_{-0.6}$	1.4	6.3	0.42/25
MECS	Jul 26, 10:12:39	Jul 27, 06:43:33	23309	0.8 ± 0.1	1.18	5.8	0.86/43
PCA	Nov 2, 10:56:16	Nov 2, 11:29:36	2000	$1.45^{+0.3}_{-0.25}$	10.3	19.7	0.45/25
MECS	Oct 31, 20:46:55	Nov 2, 09:59:28	33661	1.6 ± 0.05	12.7	19.7	0.61/58

NOTE.—The spectral analysis results for the PCA have been obtained for a fitted energy range 3–15 keV; the *BeppoSAX* MECS results have been obtained through MECS spectral analysis over the range 1–10 keV (Ravasio et al. 2003); α is the energy spectral index.

previous spectral analyses of X-ray observations of BL Lac (Sambruna et al. 1999; Madejski et al. 1999; Ravasio et al. 2002). The fit resulted in $\alpha = 0.8 \pm 0.1$. This is perfectly consistent with the result from the contemporaneous *RXTE* PCA observation. The spectral index of $\alpha = 0.8 \pm 0.1$ confirms the low-activity state of the source at that time and indicates that the entire X-ray spectrum might have been dominated by the low-frequency end of the high-energy component of the broadband SED of BL Lac.

The short-term LECS (0.7–2 keV) and MECS (2–10 keV) light curves of BL Lac during this observation (see Fig. 3 of Ravasio et al. 2003) display a large (factor of >2) flare on a timescale of $\sim$4 hr, while the source appears less variable at higher energies. This behavior has been noted in this source before (see, e.g., Ravasio et al. 2002) and is even more obvious in the October 31–November 2 observation (see § 2.3.2). The low count rate and relatively short exposure time prevents a more detailed analysis of variability features of this observation.

2.3.2. *October 31–November 2*

During the second *BeppoSAX* pointing on 2000 October 31–November 2, we measured the highest 2–10 keV flux ever observed with *BeppoSAX* from BL Lac. The LECS+MECS spectrum in the 0.3–10 keV range was well fitted with a power-law model with fixed $N_{\rm H} = 2.5 \times 10^{21}$ cm^{-2}, revealing a steep X-ray spectrum with $\alpha = 1.56 \pm 0.03$ (Ravasio et al. 2003). As for the November 26–27 observation, the spectral fitting results were consistent with the results from the PCA observations beginning $\sim$1 hr after the *BeppoSAX* pointing. In this observation, BL Lac was also significantly detected by the PDS instrument up to $\sim$50 keV. The PDS spectrum indicates a significant spectral hardening beyond $\sim$10 keV with a best-fit spectral index $\alpha_{\rm PDS} = 0.56$ for which, however, no error could be estimated because of the poor photon statistics (Ravasio et al. 2003). The soft shape of the LECS+MECS spectrum clearly indicates that it was dominated by the high-energy end of the low-energy (synchrotron) component in this observation. Evidence for the synchrotron component at soft X-ray energies had been found in BL Lac before (Madejski et al. 1999; Ravasio et al. 2002), but this is the first time that this behavior was observed extending all the way out to $\sim$10 keV. The spectral hardening evident in the PDS spectrum might indicate the onset of the high-energy component beyond $\sim$10 keV.

Figure 3 displays the LECS and MECS light curves in three different energy channels during the second *BeppoSAX* pointing, along with the two hardness ratios: HR1 = MECS (2–4)/LECS (0.5–2) and HR2 = MECS (4–10)/MECS (2–4). The LECS and MECS light curves show significant variability in all energy channels, with flux variations of factors of $\sim$3–4 on timescales down to $\sim$1–2 hr. The PDS counts were consistent with no variability (constancy probability of $\sim$96%; Ravasio et al. 2003). Ravasio et al. (2003) have calculated the normalized excess variance parameter $\sigma^2_{\rm rms}$ for the three LECS and MECS energy channels and found that $\sigma^2_{\rm rms}$ is slightly decreasing with increasing photon energy. The LECS and MECS light curves show several individual, well-resolved flares (e.g., at $\sim$29 and $\sim$49 hr; see Fig. 3). Those flares seem to suggest slightly longer rise than decay timescales, but because of the limited photon statistics, a meaningful, more quantitative assessment of light-curve asymmetries is not possible with our present data.

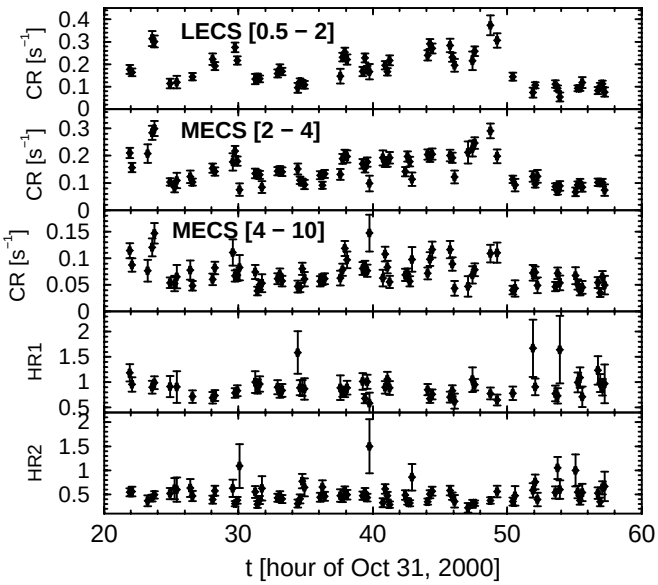

FIG. 3.—Light curves in three different energy channels of the *BeppoSAX* LECS+MECS observations on 2000 October 31–November 2. The two lower panels show the hardness ratios HR1 = MECS (2–4) / LECS (0.5–2) and HR2 = MECS (4–10) / MECS (2–4).

Ravasio et al. (2003) have defined a minimum doubling timescale $T_{\rm short}$ to quantify the energy dependence of the short-term variability timescale and found no significant trend of this quantity with photon energy. For all three LECS+MECS energy channels the minimum doubling timescales were found to be consistent with values of $\sim$6 ks. An estimate of the average rise and decay timescales in the rapid variability can be found through the width of the ACF of the light curves. We have calculated the discrete ACFs for the three LECS+MECS light curves and fitted them with an exponential. The results are plotted in Figure 4 and suggest a decreasing trend of the variability timescale with increasing photon energy, as illustrated in Figure 5. Clearly, the statistical errors on these measurements are too large to seriously constrain the functional dependence of the ACF widths on photon energy. However, in § 6 we suggest a new method to use a decreasing ACF width with increasing photon energy for an independent magnetic field estimate and apply this method to the *BeppoSAX* results, tentatively taking the best-fit results at face value.

2.4. *Gamma-Ray Observations*

BL Lac has been observed by the HEGRA system of imaging Cerenkov telescopes, accumulating a total of 10.5 hr of on-source time in 2000 September–November. The source was not detected above a 99% confidence level upper limit of 25% of the Crab flux at photon energies above 0.7 TeV (Mang et al. 2001). Assuming an underlying power law with energy spectral index α, this corresponds to a νF_ν flux limit of $8.65 \times 10^{11}\ \alpha$ Jy Hz at 0.7 TeV.

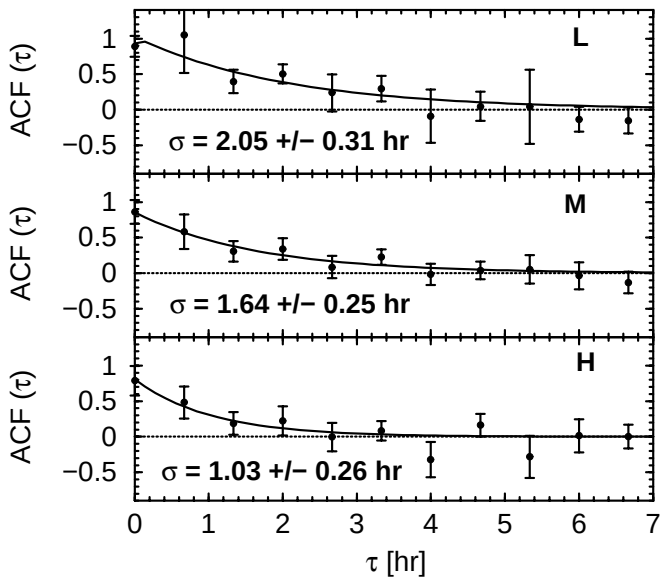

FIG. 4.—Discrete ACFs of the X-ray flux in three energy channels: L = LECS (0.5–2) keV, M = MECS (2–4) keV, and H = MECS (4–10) keV. The ACFs have been fitted with a symmetric constant+exponential; σ as quoted in the individual panels is the best-fit value of the decay time constant.

3. SPECTRAL VARIABILITY

In this section, we describe local spectral variability phenomena, i.e., the variability of local spectral (and color) indices and their correlations with monochromatic source fluxes.

3.1. *Optical Spectral Variability*

The optical spectral variability of BL Lac during our campaign has been investigated in great detail by Villata et al. (2002). In the following, we briefly summarize their results. Villata et al. (2002) have calculated the dereddened, host galaxy–subtracted $B-R$ color indices for a set of 620 observations taken by the same instrument within 20 minutes of each other, with individual errors of the B and R magnitudes of no more than 0.04 and 0.03 mag, respectively. Obvious spectral variability was detected, and the color changes were more sensitive to rapid variations than the long-term flux level. During well-sampled, short flares (on timescales of a few hours), the color changes strictly follow the flux variability, in the sense that the spectra are harder when the flux is higher (see Fig. 7 of Villata et al. 2002). A plot of $B-R$ versus R reveals two separate regimes, within which the R magnitudes are well correlated with the respective $B-R$ colors. However, there seems to be a discontinuity at $R \sim 14$ mag, separating a high-flux and a low-flux regime. Within each regime, a similar range of $B-R$ colors is observed. Villata et al. (2002) have subsequently fitted the overall long-term flux variability by a cubic spline to the 10 day averages of the R-band light curve and rescaled this spline to pass through the minima of the light curve. Cleaning the B and R fluxes from this base-flux level, they removed the long-term variability from the color-intensity correlation and found a very clean correlation between the superposed short-term R-band variability and the $B-R$ spectral hardness. This strongly suggests that the optical long-term flux variability (on timescales of weeks) is due to an achromatic mechanism, while the rapid (intraday) variability is clearly chromatic (Villata et al. 2002).

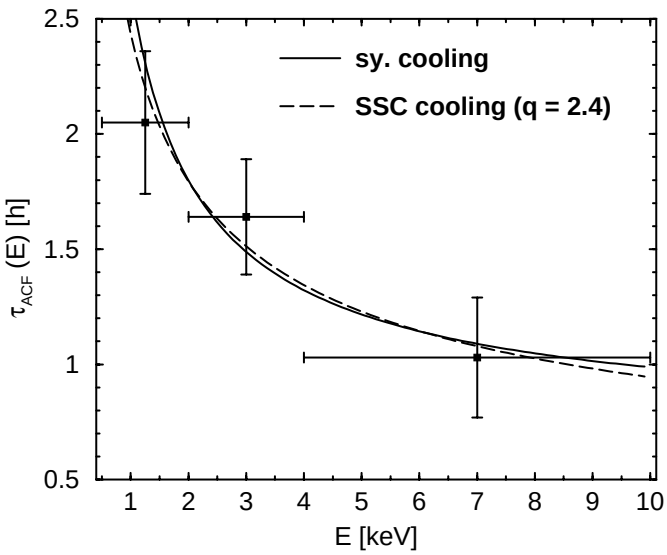

FIG. 5.—Widths of the discrete ACFs of the light curves in the LECS+MECS energy range, as a function of synchrotron photon energy. The solid curve is the best fit of this energy dependence, assuming it is caused by synchrotron+external Compton cooling; the solid curve is a fit assuming dominant SSC cooling with an injection electron spectral index of $q = 2.4$.

3.2. *X-Ray Spectral Variability*

Figure 6 displays the history of the best-fit spectral index from the *RXTE* PCA monitoring observations, along with the PCA light curve. Because of the relatively short exposure times, the errors on the spectral indices are rather large, but a general trend of the local spectral index being softer during strong hard X-ray (2–10 keV) flares is discernible. This applies to the overall low state (see, e.g., the flares at MJD 51708 = June 13 or MJD 51770 = August 14), as well as to the high state (e.g.,

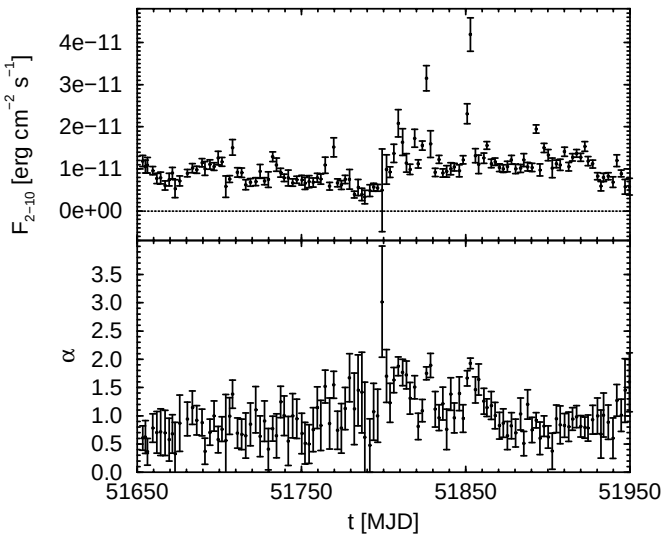

FIG. 6.—*RXTE* PCA flux and best-fit spectral-index history

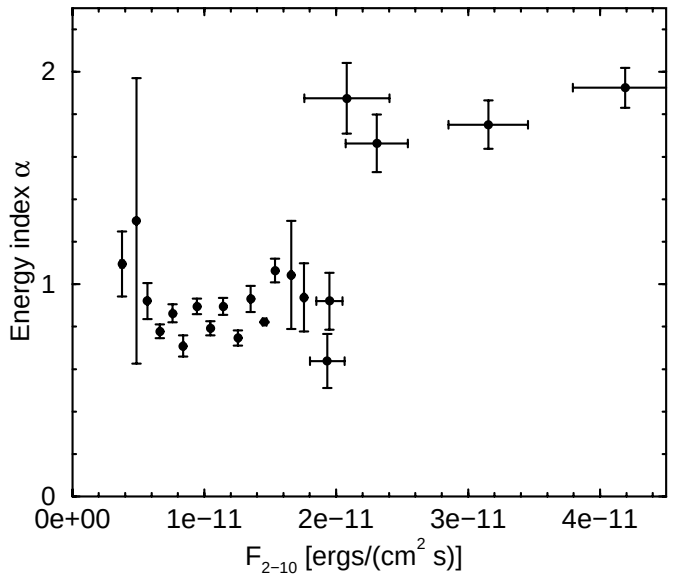

FIG. 7.—Hardness-intensity plot for the *RXTE* PCA measurements. At $F_{2-10} < 1.8 \times 10^{-11}$ ergs cm^{-2} s^{-1}, the data have been rebinned into flux bins of $\Delta F_{2-10} = 10^{-12}$ ergs cm^{-2} s^{-1}. At higher flux values, data points from individual PCA observations are displayed. High flux states are always associated with a soft spectrum, but no obvious hardness-intensity correlation is visible at low X-ray flux levels.

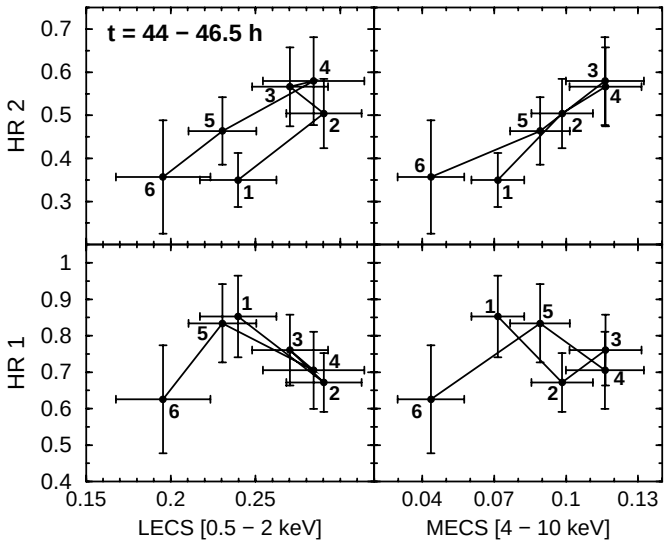

FIG. 8.—Hardness-intensity diagram of the *BeppoSAX* hardness ratios HR1 and HR2 as defined in § 2.3.2 vs. soft X-ray LECS and medium-energy MECS flux for the well-resolved X-ray flare at $t = 44.0$–46.5 hr (see Fig. 3).

MJD 51826 = October 9 or MJD 51853 = November 5). In order to investigate the question of a hardness-intensity correlation on the timescale of a few days probed by the *RXTE* monitoring, we have constructed a hardness-intensity diagram from the PCA data. To assess the average properties of the source at low fluxes, we have rebinned the points included in Figure 6 in flux bins of $\Delta F_{2-10} = 10^{-12}$ ergs cm^{-2} s^{-1} for all individual points with 2–10 keV flux of less than 1.8×10^{-11} ergs cm^{-2} s^{-1}, calculating average fluxes and spectral indices weighted by the inverse of the errors of the spectral-index measurements. Data points with larger 2–10 keV fluxes are plotted individually. The result is shown in Figure 7. The figure illustrates that high PCA 2–10 keV fluxes above $\sim 2 \times 10^{-11}$ ergs cm^{-2} s^{-1} are always characterized by soft spectra with $\alpha \geq 1$, indicating decaying νF_ν spectra. This confirms the notion mentioned above that large-amplitude X-ray flares might be dominated by the variability of the low-energy (synchrotron) component, extending into the PCA energy range during flaring activity. No significant trend of the local spectral index with X-ray flux is discernible at low X-ray flux states.

The X-ray spectral variability on short (intraday) timescales can be characterized through variations of the *BeppoSAX* hardness ratios HR1 and HR2, as defined in § 2.3.2. Their history during the second *BeppoSAX* observation on October 31–November 2 is plotted, along with the LECS and MECS light curves, in Figure 3. Considering the entire October 31–November 2 observation, we only find a very weak hint of an anticorrelation of HR1 with the soft LECS (0.5–2) keV flux and a positive correlation of HR2 with the medium-energy MECS (4–10) keV flux. These trends become slightly more apparent when following individual, well-resolved flares. Figures 8 and 9 show two examples of such hardness-intensity diagrams for the flares around 45 and 48 hr of October 31 (see Fig. 3). A weak hardness-intensity anticorrelation at soft X-rays (HR1 vs. LECS) and a positive hardness-intensity correlation at medium-energy X-rays (HR2 vs. MECS) can be seen. The flare around 48 hr also shows weak evidence for spectral hysteresis, as found previously in several HBLs, such as Mrk 421 and PKS 2155−304 (see, e.g., Takahashi et al. 1996; Kataoka et al. 2000). Such spectral hysteresis phenomena have been modeled in detail with pure synchrotron self-Compton (SSC) models for the case of HBLs (see, e.g., Kirk, Rieger, & Mastichiadis 1998; Georganopoulos & Marscher 1998; Kataoka et al. 2000; Kusunose, Takahara, & Li 2000; Li & Kusunose 2000) and recently also predicted for intermediate and low-frequency peaked BL Lac objects by Böttcher & Chiang (2002).

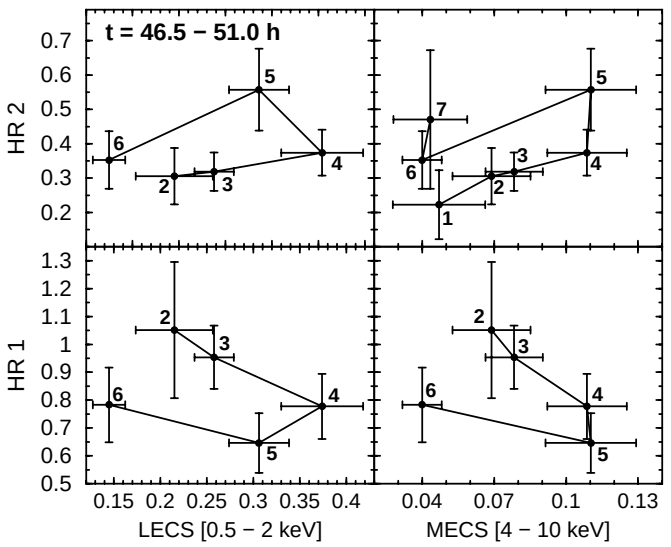

FIG. 9.—Hardness-intensity diagram of the *BeppoSAX* hardness ratios HR1 and HR2 as defined in § 2.3.2 vs. soft X-ray LECS and medium-energy MECS flux for the well-resolved X-ray flare at $t = 46.5$–51.0 hr (see Fig. 3).

4. INTERBAND CROSS-CORRELATIONS AND TIME LAGS

In this section, we investigate cross-correlations between the measured light curves at different frequencies within individual frequency bands, as well as broadband correlations between different frequency bands.

4.1. *Radio Correlations*

We have calculated the discrete correlation functions (DCFs; Edelson & Krolik 1988) between the light curves at different radio frequencies for a variety of sampling time steps $\Delta\tau$. We did not find any conclusive hints of correlations of the 37 GHz light curve with other radio light curves or light curves at other wavelength bands. This might be the result of the poor sampling of the 37 GHz light curve. Figure 10 displays the DCFs of the various radio light curves at $\nu < 22$ GHz with the 14.5 GHz light curve as reference for a sampling timescale of $\Delta\tau = 5$ days. We chose the 14.5 GHz reference light curve because it is the best-sampled radio light curve in our data set. The DCFs show evidence for a correlation between the variability at the various radio frequencies. We have subsequently fitted the DCFs with Gaussians to determine the most likely time delays between the signals at different radio frequencies. We have repeated this procedure for several other sampling timescales (specifically, $\Delta\tau = 3$ and 7 days) and found that only the result pertaining to the 14.5 versus 22 GHz DCF remained robust, indicating a time lag between the 14.5 and the 22 GHz light curves, with the 14.5 GHz light curve lagging behind the 22 GHz one by $\sim$15 days. The best fit is indicated by the solid curve in the top panel of the figure.

In order to test the statistical significance of the high-frequency radio time lag, we have performed a series of 10,000 Monte Carlo simulations, assuming uncorrelated variability patterns between the 14.5 and 22 GHz light curves. Specifically, we have simulated random light curves for the 22 GHz fluxes and performed the same DCF and Gaussian fitting analysis as we had done with the actual data. The simulated 22 GHz light curves were constrained by the measured maximum and minimum fluxes in our data set and by a short-term doubling timescale of 40 days for rapid fluctuations on $\Delta t \leq 10$ days and a long-term doubling timescale of 4 months. Simulated data points were constructed for the times of the actual 22 GHz measurements in our data set. We find a probability of 12.3% that these simulated random light curves show a DCF amplitude higher than that resulting from the real 22 GHz flux history, with an acceptable Gaussian fit to the DCF. Thus, the measured time delay cannot be considered statistically significant. This might be, at least in part, due to the fact that the data train from our campaign is relatively short.

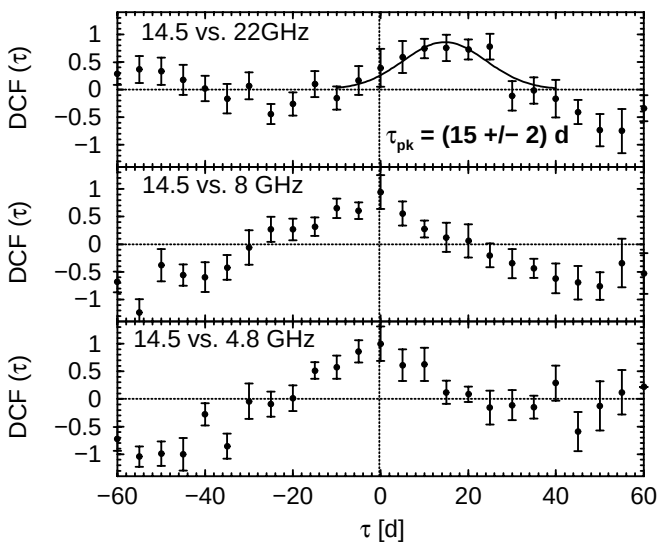

FIG. 10.—DCFs between the 14.5 GHz radio light curve (the best-sampled radio light curve available in our data set) with respect to light curves at other radio frequencies. The solid curve in the top panel indicates a Gaussian fit to the DCF, with τ_{pk} being the best-fit offset from zero (i.e., the most likely time delay). This is only included for the 14.5 vs. 22 GHz DCF, since this procedure did not produce robust results (independent of the sampling timescale) for the other DCFs shown.

4.2. *Radio-Optical Correlations*

We also calculated the DCFs between the light curves at the various radio and optical (*R*-band) light curves and calculated the best-fit time delay, as described in the previous paragraph. This resulted in low-significance detections of time delays of $\sim$45–50 days of the 8, 14.5, and 37 GHz radio light curves behind the optical ones. However, these results have to be considered with great caution, since our data set only spans about half a year. On the basis of historical data, characteristic time delays of $\sim$1–4.5 yr between the radio and optical variability had been found previously (Bregman et al. 1990). Thus, our correlations may well be a chance coincidence in the sense that the observed radio and optical variability patterns may not correspond to the same epoch of activity of the central source. A more comprehensive study of the long-term behavior of BL Lac, including the results of this multiwavelength campaign, will be the subject of subsequent work (e.g., M. Villata et al. 2003, in preparation).

As reported by Villata et al. (2002), the light curves in the different optical bands (*U*, *B*, *V*, *R*, and *I*) are well correlated (with the hardness-brightness correlation described in § 3.1), but no significant, measurable time delays between the *B* and the *R* bands (the best-sampled optical light curves in our campaign) were found.

4.3. *X-Ray–Optical Correlations*

The extraordinary time coverage of the *R*-band light curves during the core campaign allows us to do a meaningful comparison of the intraday variability patterns at optical and X-ray frequencies during our first *BeppoSAX* observation of July 26–27. Figure 11 displays the LECS 0.7–2 keV and the contemporaneous *R*-band light curve during this observation. From visual inspection, it seems that the *R*-band light curve closely tracks the LECS light curve, with a delay of $\sim$4–5 hr (indicated by the dotted arrows in Fig. 11). However, the DCF between the *R*-band flux and the LECS count rate (see Fig. 12) instead identifies a stronger apparent signal from an anticorrelation with an optical–X-ray delay of $\sim$3 hr. The dominant features probably identified by the DCF analysis are indicated by the dot-dashed arrows in Figure 11. Note that the DCF is defined so that negative τ corresponds to a lead of the X-rays. Unfortunately, the limited statistics of the *BeppoSAX* light curve prevents a more in-depth analysis of the possible optical–X-ray correlation on these short timescales. Any claimed correlation does not hold up to a

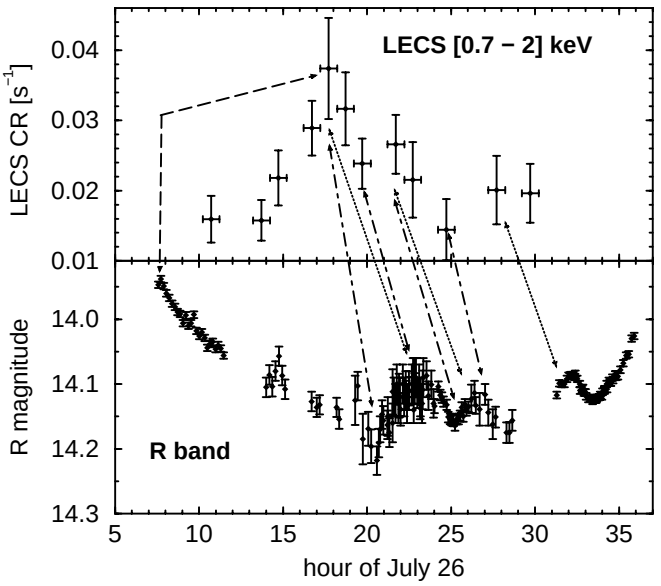

FIG. 11.—*BeppoSAX* LECS [0.7–2] keV (*top panel*) and contemporaneous *R*-band (*bottom panel*) light curves during our first *BeppoSAX* pointing on July 26–27. The optical light curve appears to trace the X-ray light curve with a time delay of ~4–5 hr, as indicated by the dotted arrows. However, a DCF analysis (see Fig. 12) actually finds a stronger signal from an apparent anticorrelation with a time delay of ~3 hr, dominated by features indicated by the dot-dashed arrows, as well as a strong positive correlation with an X-ray lag of ~9 hr behind the optical, dominated by the large optical and X-ray flares indicated by the long-dashed arrow.

statistical significance test. However, if we assume that the optical lag of ~4–5 hr is real and can be interpreted as due to synchrotron cooling, it allows an independent magnetic field estimate, which is quantified in § 6. Interestingly, the resulting magnetic field is in good agreement with an independent estimate from a basic equipartition argument.

The DCF also identifies a strong apparent correlation between optical and X-ray fluxes, with an *R*-band lead of ~9 hr, which seems to arise from the large optical flare at ~8 hr, preceding the LECS flare at ~17 hr (see the long-dashed arrows in Fig. 11). However, we believe that this might be an artifact due to the limited duration and time resolution of the LECS light curve. Note that this 9 hr timescale spans more than about half the duration of the entire *BeppoSAX* LECS light curve for this observation. We have also looked for correlations between the *R* band and X-ray fluxes on longer timescales, applying the DCF analysis to the *RXTE* PCA, ASM (daily averages), and *R*-band light curves. No significant time delays were detected.

We have also investigated possible time delays between the different *BeppoSAX* LECS and MECS light curves displayed in Figure 3 for the October 31–November 2 observation. While the DCFs show evidence for a positive correlation between all of these light curves, no measurable time delays could be identified.

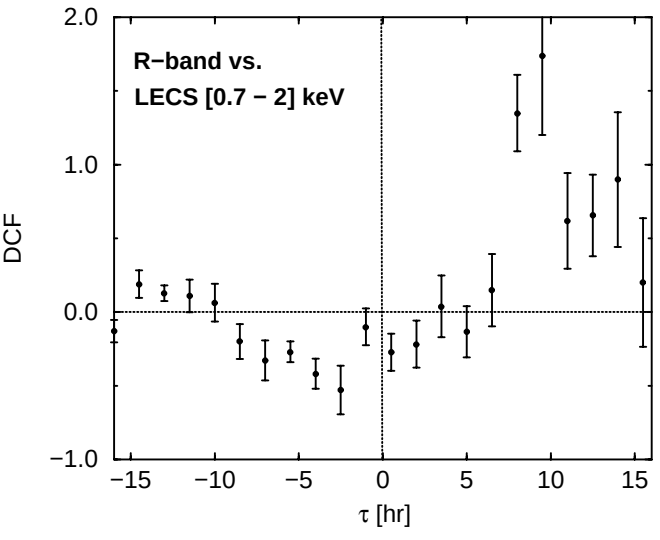

FIG. 12.—DCF between the *BeppoSAX* LECS 0.7–2 keV and *R*-band light curves during our first *BeppoSAX* pointing on July 26–27, as shown in Fig. 11. The sampling timescale is $\Delta\tau = 1.5$ hr. The same general features are found for other sampling timescales in the range of ~1–2 hr.

5. BROADBAND SPECTRAL ENERGY DISTRIBUTIONS

We have constructed simultaneous broadband SEDs for the times of the two *BeppoSAX* pointings. They are shown in Figure 13. For the radio fluxes, we selected the measurements closest in time to the center of the respective *BeppoSAX* exposures. We generally had multiple optical flux measurements throughout the times of the *BeppoSAX* exposures. To construct the SEDs, we have calculated the average optical flux in each band from the dereddened, host galaxy–subtracted individual flux measurements (see § 2.2) over the *BeppoSAX* exposure time, and we indicate the (in some cases rather substantial) range of variability over that period by the error bars on the optical fluxes.

We represent the best-fit power-law spectra of the *BeppoSAX* LECS+MECS measurements, as well as the simultaneous or quasi-simultaneous *RXTE* PCA measurements as bow-tie outlines in the SEDs. For orientation

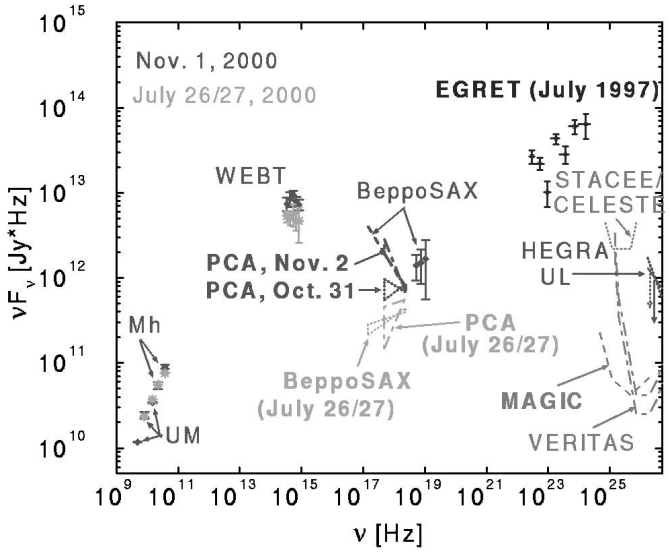

FIG. 13.—SEDs of BL Lac on 2000 July 26–27 (*light gray stars*), and 2000 October 31–November 2 (*dark gray diamonds*). For October 31–November 2, both the PCA measurement a few hours before the *BeppoSAX* pointing and near the end of the *BeppoSAX* pointing are included. "Mh" indicates the radio fluxes measured at Metsähovi Radio Observatory; "UM" indicates the University of Michigan Radio Observatory measurements. The two VERITAS sensitivity limits have been obtained assuming two different values of the underlying spectral index, $\alpha = 2.5$ and 3.5, respectively. [*See the electronic edition of the Journal for a color version of this figure.*]

purposes only, we also indicate the EGRET flux from the major gamma-ray outburst of BL Lac in 1997 July (Bloom et al. 1997). Included are also the anticipated sensitivity limits of current and future atmospheric Cerenkov telescope facilities and the HEGRA upper limit from the observations in 2000 September – November.

Figure 13 illustrates the drastically different activity states between the July 26–27 and the October 31–November 2 *BeppoSAX* observations. In the July 26–27 SED, the synchrotron peak appears to be located at frequencies clearly below the optical range (probably at $\nu_{\rm sy} \sim 10^{14}$ Hz), and the synchrotron emission cuts off at a frequency near or below $\sim 10^{17}$ Hz. In contrast, the SED of October 31–November 2 shows clear evidence for the presence of the synchrotron component out to at least 10 keV, and the synchrotron peak might be located in the optical range at a few times 10^{14} Hz. For purposes of illustration, we have also plotted the *RXTE* PCA spectrum of the observation a few hours before the beginning of the October 31–November 2 *BeppoSAX* pointing. This PCA spectrum shows characteristics rather similar to those of the low-state spectrum and illustrates the drastic nature of the short-term X-ray variability. This might indicate that the rapid variability of BL Lac is probably driven by short episodes of injection/acceleration of high-energy electrons into the emitting volume.

Ravasio et al. (2003) have shown that the extrapolation of the optical spectrum toward higher frequencies does not connect smoothly with the contemporaneous soft X-ray spectrum (see their Fig. 5). They have considered various possible explanations of this discrepancy: (1) a variable dust-to-gas ratio, which could cause a larger degree of reddening during the October 31–November 2 observations, (2) the bulk Compton process (Sikora et al. 1997), which could provide an additional emission component at soft X-rays due to Compton upscattering of external photons by a thermal component of electrons in the emitting volume, (3) a second component of relativistic electrons, providing an additional source of synchrotron emission at soft X-rays, and (4) the flattening effect of the Klein-Nishina cutoff on the cooling electron distribution, leading to a high-energy bump in the synchrotron emission (see Dermer & Atoyan 2002 for a recent application of this idea to the optical–X-ray spectra of individual knots in jets of radio galaxies detected by *Chandra*). While the first two of the ideas listed above were found to lead to rather unrealistic inferences about the environment of the AGN and the underlying accretion-disk spectrum, respectively, the latter two scenarios will be considered further in our modeling efforts in our companion theory paper (M. Böttcher & A. Reimer 2003, in preparation). However, it also seems possible that this misalignment could be an artifact of the flux averaging over the $\sim$1.5 days of the *BeppoSAX* observations, including multiple short-term flares of only a few hours each. In order to test for this possibility, it will be essential to use a fully time-dependent AGN emission model and do the flux averaging in a way similar way to that used to construct the SEDs displayed in Figure 13.

6. GENERIC PARAMETER ESTIMATES

In this section, we discuss some general constraints on source parameters that will be relevant for detailed spectral and variability modeling of BL Lac. We first (§ 6.1) focus on three independent methods to estimate the magnetic field and then turn to other properties, such as the comoving Lorentz factors of electrons in the jet, the bulk Lorentz and Doppler boosting factors, the kinetic luminosity of the jet, and the source size.

6.1. *The Magnetic Field*

In § 2.3, we had investigated the energy-dependent width of the ACFs of the X-ray variability during the October 31–November 2 *BeppoSAX* observation (see Fig. 5). Assuming that the rise time of short-term flaring is not significantly dependent on energy (i.e., it is dominated by light-crossing time constraints rather than an energy-dependent acceleration timescale), the width of the ACF should yield an estimate of the cooling timescale $\tau_c(E)$ of the electrons responsible for the emission at energy E as a function of photon energy. Specifically, in that case, we expect that $\tau_{\rm ACF}(E) = \tau_0 + \tau_c(E)$. If the LECS+MECS spectrum is indeed dominated by synchrotron emission, we can associate an observed photon energy $E = 1 E_{\rm keV}$ keV with the characteristic photon energy of synchrotron-emitting electrons, $E_{\rm keV} = 1.4 \times 10^{-11} D B_{\rm G} \gamma^2$, where $B = 1 B_{\rm G}$ G is the comoving magnetic field and γ is the electron Lorentz factor. If the electron cooling is dominated by synchrotron and/or external Compton (EC) cooling in the Thomson regime, we have $\dot{\gamma} = -(4/3)\, c\, \sigma_{\rm T}\, (u_B/m_e c^2)\, (1+k)\, \gamma^2$, where u_B is the energy density in the magnetic field and $k \equiv u_{\rm ext}/u_B$ is the ratio of the energy density in an external photon field to the magnetic field energy density (all quantities in the comoving frame of the emitting region). This yields the synchrotron+EC cooling time (in the observer's frame) of

$$\tau_{\rm cool,sy}(E) = 2.9 \times 10^3 D^{-1/2} B_{\rm G}^{-3/2}\, (1+k)^{-1}\, E_{\rm keV}^{-1/2}\ {\rm s}\ . \quad (1)$$

Fitting a function $\tau_{\rm ACF}(E) = \tau_0 + \tau_1\, E_{\rm keV}^{-1/2}$ to the energy dependence shown in Figure 5 (*solid line*) yields a best-fit value of $\tau_1 = 7800 \pm 1400$ s, which implies

$$B = (0.24 \pm 0.03) D_1^{-1/3} (1+k)^{-2/3}\ {\rm G}\ ,$$

where $D_1 = D/10$.

Alternatively, if electron cooling is dominated by the SSC process, the relevant photon field energy density is $u_{\rm sy}$, which we can approximate as

$$u_{\rm sy} \approx \tau_{\rm T} u_B \frac{q-1}{3-q} \gamma_1^{q-1} \gamma_2^{3-q}\ , \quad (2)$$

where $\tau_{\rm T} = n_e \sigma_{\rm T} R_B$ is the radial Thomson depth of the emitting region and q is the spectral index of the *injected* electron spectrum, $Q(\gamma) = Q_0 \gamma^{-q}$ for $\gamma_1 \le \gamma \le \gamma_2$. The decay timescale of the light curve at a characteristic synchrotron photon energy E will then correspond to the Compton cooling timescale of electrons at the high-energy end of the electron spectrum, γ_2, at the time when their characteristic synchrotron frequency equals E. Thus, the relevant cooling rate is

$$\frac{d\gamma_2}{dt} = -\frac{4}{3} c \sigma_{\rm T} \frac{U_B}{m_e c^2} \frac{q-1}{3-q} \tau_{\rm T} \gamma_1^{q-1} \gamma_2^{5-q}\ . \quad (3)$$

This yields a characteristic cooling time (in the observer's frame) of

$$\tau_{\rm cool,SSC} = 7.7 \times 10^8 \frac{3-q}{q-1} (2.4 \times 10^5)^{q-4} \tau_{\rm T}^{-1} \gamma_1^{1-q} B_{\rm G}^{-q/2} \times D^{(2-q)/2} E_{\rm keV}^{(q-4)/2}\ {\rm s}\ . \quad (4)$$

Leaving the index q free, we find a best-fit energy dependence of $\tau_{\rm cool} = \tau_0 + \tau_1 E_{\rm keV}^{-\zeta}$ with $\zeta = 0.50 \pm 0.14$, which yields the same energy dependence as in the synchrotron-cooling case. However, the optical spectral index of $\alpha_o \sim 1.2$ corresponds to a time-averaged (or equilibrium in the case of a balance between particle injection and radiative cooling) electron spectral index of $p = 3.4$, indicating a value of $q = 2.4$. Fixing $q = 2.4$ (i.e., $\zeta = 0.8$), the fit is still perfectly consistent with the measured energy dependence, as indicated by the dashed line in Figure 5. From the best-fit value of $\tau_1 = 7020 \pm 1980$ s, we can derive a magnetic field estimate of $B = (0.20 \pm 0.05)\tau_{\rm T,-6}^{-5/6}(\gamma_1/100)^{-7/6} D_1^{-1/12}$ G. With the available data, the two cooling scenarios can obviously not be distinguished, and the estimates may be rather uncertain because of the possible effect of energy-dependent acceleration times and energy-dependent photon propagation times through the blob. Thus, our magnetic field estimates based on equations (1) and (4) are meant as a suggestion for the analysis of higher quality data from future observations by X-ray observatories with higher throughput, like *Chandra*, *XMM-Newton*, or the planned Constellation-X mission, rather than as a realistic magnetic field estimate from our currently available *BeppoSAX* data.

Another independent magnetic field estimate could be obtained from the time delay between the *BeppoSAX* LECS 0.7–2 keV and the *R*-band light curves of $\Delta t^{\rm obs} \sim 4$–5 hr, for which Figure 11 shows tantalizing, although not statistically significant, support. Assuming that the correlation is real and the delay is caused by synchrotron cooling of high-energy electrons with characteristic observed synchrotron photon energy $E_{\rm sy,0} = E_0$ keV to lower energies with corresponding synchrotron energy $E_{\rm sy,1} = E_1$ keV, we find a magnetic field estimate analogous to equation (1):

$$B_{\rm delay} = 0.4 D_1^{-1/3}(1+k)^{-2/3}(\Delta t_h^{\rm obs})^{-2/3} \times (E_1^{-1/2} - E_0^{-1/2})^{2/3} \ {\rm G}\ , \quad (5)$$

where $\Delta t_h^{\rm obs}$ is the observed time delay in hours. Using $\Delta t_h^{\rm obs} = 5$, $E_0 = 1$ for the LECS, and $E_1 = 5.6 \times 10^{-4}$ for the *R* band, we find

$$B_{\rm delay,RX} = 1.6 D_1^{-1/3}(1+k)^{-2/3} \ {\rm G}\ . \quad (6)$$

We need to point out that equation (6) may, in fact, slightly overestimate the actual magnetic field, since at least the optical synchrotron emitting electrons may also be affected by adiabatic losses and escape. Depending on the details (geometry and mechanism) of the jet collimation, those processes can act on timescales as short as the dynamical timescale, which is constrained by the observed minimum variability timescale of $\Delta t_{\rm dyn} \lesssim 1.5$ hr (in the observer's frame). Another note of caution that needs to be kept in mind is that the rather large sampling timescale of the X-ray light curve of $\Delta t = 1$ hr precludes the estimation of magnetic fields larger than $B_{\rm delay,max} \sim 4.8 D_1^{-1/3}(1+k)^{-2/3}$ G from delays between the optical and X-ray light curves. Consequently, magnetic fields larger than $B_{\rm delay,max}$ cannot be excluded on the basis of the present analysis.

In principle, one could also derive an analogous estimate for the SSC-cooling case. However, it is unlikely that SSC cooling can dominate when the bulk of the synchrotron emission has evolved down to optical frequencies. Thus, it would not be realistic to apply such an estimate to the optical–X-ray time delay.

A third independent estimate of the comoving magnetic field can be found by assuming that the dominant portion of the time-averaged synchrotron spectrum is emitted by a quasi-equilibrium power-law spectrum of electrons with $N_e(\gamma) = n_0 V_B \gamma^{-p}$ for $\gamma_1 \le \gamma \le \gamma_2$; here V_B is the comoving blob volume. The normalization constant n_0 is related to the magnetic field through an equipartition parameter $e_B \equiv u_B/u_e$ (in the comoving frame). Note that this equipartition parameter only refers to the energy density of the electrons, not accounting for a (possibly greatly dominant) energy content of a hadronic matter component in the jet. Under these assumptions, the νF_ν peak synchrotron flux $f_\epsilon^{\rm sy}$ at the dimensionless synchrotron peak energy $\epsilon_{\rm sy}$ is approximately given by

$$f_\epsilon^{\rm sy} = (DB)^{7/2} \frac{\pi c \sigma_{\rm T}}{288 d_L^2} \left[(1+z)\epsilon_{\rm sy} B_{\rm cr}\right]^{1/2} \frac{p-2}{e_B m_e c^2}\ , \quad (7)$$

where $B_{\rm cr} = 4.414 \times 10^{13}$ G. Note that the electron spectrum normalization used to derive equation (7) is based on the synchrotron spectrum above the synchrotron peak, where the underlying electron spectrum always has an index of $p \ge 3$. Equation (7) yields a magnetic field estimate of

$$B_{e_B} = 9 D_1^{-1} \left[\frac{d_{27}^4 f_{-10}^2 e_B^2}{(1+z)^4 \epsilon_{\rm sy,-6} R_{15}^6 (p-2)}\right]^{1/7} {\rm G}\ , \quad (8)$$

where $f_{-10} = f_\epsilon^{\rm sy}/(10^{-10}$ ergs cm^{-2} s$^{-1})$, $\epsilon_{\rm sy,-6} = \epsilon_{\rm sy}/10^{-6}$, and $R_{15} = R_B/(10^{15}$ cm). With $d_{27} = 0.87$, $f_{-10} = 1$, $\epsilon_{\rm sy,-6} = 4$, $R_{15} = 2$, and $p = 3.4$, this yields

$$B_{e_B} = 3.6 D_1^{-1} e_B^{2/7} \ {\rm G}\ . \quad (9)$$

This is in excellent agreement with the estimate from the X-ray–optical delay, if the Doppler factor is slightly larger than 10 and/or the magnetic field equipartition parameter is slightly less than 1. We thus conclude that a magnetic field of $B \sim 2 e_B^{2/7}$ G might be a realistic value for BL Lac. We point out that the estimates in equations (5) and (8) should be valid for any model that represents the low-energy component of the blazar SED as synchrotron emission from relativistic electrons, which is the case for virtually all variations of leptonic and hadronic jet models.

6.2. *Other Relevant Parameters*

Based on the magnetic field estimate of 1.5–2 G, the approximate location of the synchrotron peak of the SEDs of BL Lac at $\nu_{\rm sy} \sim 10^{14}$ Hz allows us to estimate that the electron energy distribution in the synchrotron-emitting region should have a peak at $\langle\gamma\rangle \sim 1.4 \times 10^3 D_1^{-1/2}$. The location of the synchrotron cutoff in the quiescent state at $\nu_{\rm sy,co}^{\rm qu} \lesssim 10^{17}$ Hz then yields a maximum electron energy in the quiescent state of $\gamma_2^{\rm qu} \lesssim 4 \times 10^4 D_1^{-1/2}$, while the synchrotron cutoff in the flaring state at $\nu_{\rm sy,co}^{\rm fl} \sim 2.4 \times 10^{18}$ Hz yields $\gamma_2^{\rm fl} \sim 2 \times 10^5 D_1^{-1/2}$.

The superluminal motion measurements mentioned in the introduction place a lower limit on the bulk Lorentz factor of $\Gamma \gtrsim 8$, and we expect that the Doppler boosting factor D is of the same order. Since, unfortunately, we only have upper limits on the VHE gamma-ray flux during our campaign, and no measurements in the MeV–GeV regime, no independent estimate from $\gamma\gamma$ opacity constraints can be derived. However, such an estimate was possible for the 1997 July gamma-ray outburst and yielded $D \gtrsim 1.4$

(Böttcher & Bloom 2000), which is a much weaker constraint than derived from the superluminal motion observations. From the optical and X-ray variability timescale, we find an upper limit on the source size of $R_B \lesssim 1.6 \times 10^{15} D_1$ cm.

If the electrons in the jet are efficiently emitting most of their comoving kinetic energy before escaping the emission region (fast-cooling regime), then the kinetic luminosity of the leptonic component of the jet would have to be $L_j^e \gtrsim 4\pi\, d_L^2\, (\nu F_\nu)^{\rm pk}/D^4 \sim 10^{41} D_1^{-4}$ ergs s^{-1}. If the electrons are in the slow-cooling regime (i.e., they maintain a substantial fraction of their energy before escaping the emitting region) and/or the jet has a substantial baryon load (for a recent discussion see, e.g., Sikora & Madejski 2000), the kinetic energy of the jet would have to be accordingly larger.

In both leptonic and hadronic blazar models, one needs an estimate of the energy density in the external photon field. In the case of leptonic models, this determines the external Compton processes, in hadronic models, $p\gamma$ processes on external photons depend on this quantity. For this purpose, an estimate of the average distance of the BLR from the central engine is needed, which can be achieved in the following way. The most recent determination of the mass of the central black hole in BL Lac can be found in Wu & Urry (2002). They find a value of $M_{\rm BH} = 1.7 \times 10^8\ M_\odot$. Then, if the width of the emission lines measured by Vermeulen et al. (1995) and Corbett et al. (1996, 2000) is interpreted as due to Keplerian motion of the BLR material around the central black hole, we find an estimate of the average distance of the line-producing material of $\bar{r}_{\rm BLR} \sim 4.7 \times 10^{-2}$ pc.

All of these estimates are model-independent and provide a generic framework for all relativistic jet models (in particular, leptonic as well as hadronic models) aimed at reproducing the broadband SEDs and variability of BL Lac during our campaign.

7. SUMMARY

We have presented the observational results of an extensive multiwavelength monitoring campaign on BL Lac in the second half of 2000. The campaign consisted of simultaneous or quasi-simultaneous observations at radio, optical, and X-ray frequencies. Also, a simultaneous upper limit at greater than 0.7 TeV was obtained with the HEGRA atmospheric Cerenkov telescope facility. We have presented light curves, spectral variability characteristics, and broadband SEDs of BL Lac during our observations. We have also looked for cross-correlations and time lags between different frequency bands, as well as between narrow energy bands within the same frequency bands.

The WEBT optical campaign achieved an unprecedented time coverage, virtually continuous over several 10–20 hr segments. It revealed intraday variability on timescales of $\sim$1.5 hr and evidence for spectral hardening associated with increasing optical flux. The multiwavelength campaign included two $\sim$25–30 ks pointings with the *BeppoSAX* satellite.

During the campaign, BL Lac underwent a major transition from a rather quiescent state prior to 2000 September to a long-lasting flaring state throughout the rest of the year. This was also evident in the X-ray activity of the source. The *BeppoSAX* observations on July 26–27 revealed a rather low X-ray flux and a hard spectrum, while a *BeppoSAX* pointing on 2000 October 31–November 2, indicated significant variability on timescales of $\lesssim$a few hours and provided evidence for the synchrotron spectrum extending out to $\sim$10 keV during that time.

Details of the data analyses, as well as results pertaining specifically to the optical and X-ray observations, have been published in two previous papers on this campaign (Villata et al. 2002; Ravasio et al. 2003). The new results presented in this paper for the first time include the following:

1. We found a weak, low-significance indication of a delay of the 14.5 GHz light curve behind the 22 GHz light curve of $\sim$15 days. No significant delays between the 14.5 GHz light curve and the lower frequency light curves on the timescales covered by our campaign ($\lesssim \frac{1}{2}$ yr) were detected.
2. We found that the optical intraday variability during the first *BeppoSAX* observation on July 26–27 seems to trace the soft X-ray variability, with a time delay of $\sim$4–5 hr. If this delay is real and the result of synchrotron cooling of ultrarelativistic electrons, we can derive a magnetic field estimate of $B_{\rm delay,RX} = 1.6 D_1^{-1/3} (1+k)^{-2/3}$ G.
3. An additional, model-independent estimate of the magnetic field in the BL Lac jet system from equipartition arguments yielded $B_{e_B} = 3.6 D_1^{-1} e_B^{2/7}$ G.
4. We suggested a new method to estimate the magnetic field from the width of the ACF of light curves at different photon energies, assuming that differences in the ACF widths are a measure of the energy-dependent radiative cooling timescale. In the case of the data available from our campaign, this energy dependence is poorly constrained. However, taking the best-fit parameters at face value, we demonstrate our new method and find magnetic field estimates that are somewhat lower than inferred from the optical–X-ray delay and from the equipartition argument.
5. We investigated the correlation between X-ray spectral hardness and intensity. The *RXTE* PCA data show a general trend of spectral softening during the highest flux states on the timescale of several days sampled by those observations. For the second *BeppoSAX* observation, we could isolate individual short-term flares of a few hours and plot hardness-intensity diagrams over those individual flares. At soft X-rays, we confirm the general trend of spectral softening during flares, while the medium-energy X-rays show the opposite trend. In addition, some (although not all) short-term flares show weak evidence for X-ray spectral hysteresis.

Our campaign has revealed an extremely rich phenomenology of X-ray spectral variability features that provides great potential for a deeper understanding of the nature and energetics of the jets of low-frequency peaked and intermediate BL Lac objects. However, the detection of these spectral variability phenomena were at (or even beyond) the limits of the capabilities of the *BeppoSAX* instruments. We strongly encourage future observations with the new generation of X-ray telescopes, in particular *Chandra* and *XMM-Newton*, to provide a more reliable and detailed study of these X-ray spectral variability phenomena.

Detailed modeling of the SEDs and variability properties of BL Lac measured during this campaign will be presented in a companion paper (M. Böttcher & A. Reimer 2003, in preparation).

We thank the anonymous referee for a very quick review with very useful comments, which have helped to clarify and

improve the paper. We also thank A. Reimer for a careful reading of the manuscript and very useful suggestions. A. P. Marscher, S. G. Jorstad, and M. F. Aller were supported in part by NASA through grant NAG 5-11811. The work of M. Ravasio and G. Tagliaferri was supported by the Italian Ministry for University and Research. The work of M. Villata and C. M. Raiteri was supported by the Italian Space Agency (ASI) under contract CNR-ASI 1/R/073/02. The European Institutes belonging to the ENIGMA collaboration acknowledge EC funding under contract HPRN-CT-2002-00321. The St. Petersburg group was supported by federal programs "Astronomy" (grant 40.022.1.1.1001) and "Integration" (grant B0029). A. Sadun and M. Kelly would like to thank the faculty and staff at UC Boulder's Sommers-Bausch Observatory for the generous opportunity to use their facilities.

REFERENCES

Aharonian, F., et al. 2000, A&A, 353, 847
———. 2002, A&A, 384, L23
Bloom, S. D., et al. 1997, ApJ, 490, L145
Böttcher, M. 2002, in XXIInd Moriond Astrophysics Meeting, The Gamma-Ray Universe, ed. A Goldwurm, D. Neumann, & J. Trân Thanh Vân (Hanoi: Thê Giói), 151
Böttcher, M., & Bloom, S. D. 2000, AJ, 119, 469
Böttcher, M., & Chiang, J. 2002, ApJ, 581, 127
Böttcher, M., Mukherjee, R., & Reimer, A. 2002, ApJ, 581, 143
Bregman, J. N., et al. 1990, ApJ, 352, 574
Cardelli, M. T., Clayton, G. C., & Mathis, J. S. 1989, ApJ, 345, 245
Carini, M. T., Miller, H. R., Noble, J. C., & Goodrich, B. D. 1992, AJ, 104, 15
Catanese, M., et al. 1998, ApJ, 501, 616
Chadwick, P. M., et al. 1999, ApJ, 513, 161
Clements, S. D., & Carini, M. T. 2001, AJ, 121, 90
Corbett, E. A., Robinson, A., Axon, D. J., & Hough, J. H. 2000, MNRAS, 311, 485
Corbett, E. A., et al. 1996, MNRAS, 281, 737
de Jager, O., & Stecker, F. W. 2002, ApJ, 566, 738
Denn, G. R., Mutel, L. R., & Marscher, A. P. 2000, ApJS, 129, 61
Dermer, C. D., & Atoyan, A. M. 2002, ApJ, 568, L81
Edelson, R. A., & Krolik, J. H. 1988, ApJ, 333, 646
Georganopoulos, M., & Marscher, A. P. 1998, ApJ, 506, L11
Hartman, R. C., et al. 1999, ApJS, 123, 79
Holder, J., et al. 2003, ApJ, 583, L9
Horan, D., et al. 2002, ApJ, 571, 753
Kataoka, J., Takahashi, T., Makino, F., Inoue, S., Madejski, G. M., Tashiro, M., Urry, C. M., & Kubo, H. 2000, ApJ, 528, 243
Kirk, J. G., Rieger, F. M., & Mastichiadis, A. 1998, A&A, 333, 452
Krawczynski, H., Coppi, P. S., & Aharonian, F. A. 2002, MNRAS, 336, 721
Kusunose, M., Takahara, F., & Li, H. 2000, ApJ, 536, 299
Li, H., & Kusunose, M. 2000, ApJ, 536, 729
Madejski, G., et al. 1999, ApJ, 521, 145
Mang, O., et al. 2001, in Proc. 27th Int. Cosmic-Ray Conf. (Hamburg), 2658
Mattox, J. R., Hartman, R. C., & Reimer, O. 2001, ApJS, 135, 155
Miller, H. R., Carini, M. T., & Goodrich, B. D. 1989, Nature, 337, 627
Mücke, A., & Protheroe, R. J. 2001, Astropart. Phys., 15, 121
Mücke, A., Protheroe, R. J., Engel, R., Rachen, J. P., & Stanev, T. 2003, Astropart. Phys., 18, 593
Nesci, R., Maesano, M., Massaro, E., Montagni, F., Tosti, G., & Fiorucci, M. 1998, A&A, 332, L1
Neshpor, Y. I., Chalenko, N. N., Stepanian, A. A., Kalekin, O. R., Jogolev, N. A., Fomin, V. P., & Shitov, V. G. 2001, Astron. Rep., 45, 249
Punch, M., et al. 1992, Nature, 358, 477
Quinn, J., et al. 1996, ApJ, 456, L83
Raiteri, C. M., et al. 2001, A&A, 377, 396
Ravasio, M., Tagliaferri, G., Ghisellini, G., Tavecchio, F., Böttcher, M., & Sikora, M. 2003, A&A, in press
Ravasio, M., et al. 2002, A&A, 383, 763
Ryter, C. E. 1996, Ap&SS, 236, 285
Sambruna, R., et al. 1999, ApJ, 515, 140
Schlegel, D. J., Finkbeiner, D. P., & Davis, M. 1998, ApJ, 500, 525
Sikora, M., & Madejski, G. 2000, ApJ, 534, 109
Sikora, M., Madejski, G., Moderski, R., & Poutanen, J. 1997, ApJ, 484, 108
Speziali, R., & Natali, G. 1998, A&A, 339, 382
Takahashi, T., et al. 1996, ApJ, 470, L89
Vermeulen, R. C., Ogle, P. M., Tran, H. D., Browne, I. W. A., Cohen, M. H., Readhead, A. C. S., Taylor, G. B., & Goodrich, R. W. 1995, ApJ, 452, L5
Villata, M., et al. 2000, A&A, 363, 108
———. 2002, A&A, 390, 407
Weekes, T. C., et al. 2002, Astropart. Phys., 17, 221
Wu, J. H., & Urry, C. M. 2002, ApJ, 579, 530